Hydro-frac Monitoring Using Ground Time-domain EM

G. Michael Hoversten [1]

Michael Commer [2]

Eldad Haber[3]

Christoph Schwarzbach[3]

Chevron Energy Technology Company [1]

Lawrence Berkeley National Laboratory [2]

University of British Columbia[3]

Presented at the 2014 EAGE Conference, Amsterdam Netherlands, June 16

Workshop 09 CSEM: Where Do We Stand and Where Can We Go?

Abstract

As motivation for considering new electromagnetic techniques for hydraulic fracture monitoring we develop a simple financial model for the net present value offered by geophysical characterization to reduce the error in stimulated reservoir volume calculations. This model shows that even a 5% improvement in stimulated reservoir volume for a 1 billion barrel (bbl.) field results in over 1 billion US dollars (US$) in net present value over 24 years for $100/bbl oil and 0.5 billion US dollars for $50/bbl oil. The application of conductivity upscaling, often used in electromagnetic modeling to reduce mesh size and thus runtimes, is shown to be inaccurate for the high electrical contrasts needed to represent steel cased wells in the earth. Fine scale finite-difference modeling with 12.22 mm cells to capture the steel casing and fractures shows that the steel casing provides a direct current pathway to a created fracture that significantly enhances the response compared to neglecting the steel casing. We consider conductively enhanced proppant, such as coke-breeze coated sand, and a highly saline brine solution to produce electrically conductive fractures. For a relatively small frac job at a depth of 3 km, involving 5000 bbl. of slurry and a source midpoint to receiver separation of 50m, the models show that the conductively enhanced proppant produces a 15% increase in the electric field strength (in-line with the transmitter) in a 10 Ωm background. In a 100 Ωm background, the response due to the proppant increases to 213 %. Replacing the conductive proppant by brine with a concentration of 100,000 PPM NaCl, the field strength is increased by 23% in the 100 Ωm background and 2.3% in the 10 Ωm background. All but the 100,000 PPM NaCl brine in a 10 Ωm background produce calculated fracture-induced electric field increases that are significantly above 2%, a value that has been observed in field measurements.

Introduction

Hydraulic fracturing of reservoirs has been used in the hydrocarbon industry for over fifty years. With the recent onset of high production from unconventional reservoirs, its use has significantly increased. Efficient production of hydraulically fractured reservoirs requires accurate prediction of the extent and active surface area of fractures or fracture networks that are created and/or activated. Micro-earthquake (MEQ) surveys are often applied to locate the occurrence of fractures and have become critical input to discrete fracture models (DFM). Coupled geomechanical modelling and flow simulation in MEQ derived DFM models are used to predict stimulated reservoir volume (SRV). MEQ event locations are critically dependent on the velocity model used. SRV estimates can change dramatically when velocity models are

updated. Even when MEQ event locations are accurate, by themselves MEQ events cannot tell if injected proppant has reached the MEQ event locations or if fractures associated with MEQ events are connected to the well bore. Additionally, existing fractures which may open and accept proppant may not produce a measureable MEQ event. Thus the SRV estimates which are critical for optimal well placement as well as reserve estimates can be extremely uncertain.

EM methods can play an important role in improving fracture models used in simulation because they can sense where fluid and conductively enhanced proppant actually go. Single-borehole EM logging and crosswell EM imaging are available, but have limited spatial coverage dictated by well locations. Surface techniques are more economic and can provide increased spatial coverage of resistivity variations, which can be related to proppant distribution if a conductively enhanced proppant is used.

This paper explores the sensitivity of a surface based time domain electromagnetic systems for monitoring hydraulic fractures (hydro-frac). Typical proppant slurries can have electrical resistivity close to brine which in some circumstances can provide enough of a resistivity contrast with the formation to image with electromagnetic (EM) techniques. However, conductively enhanced proppant mixtures can significantly increase the resistivity contrast between the slurry filled fracture and the formation and thus enhance the ability of an EM technique to detect and map the fractures. Recently, Pardo and Torres-Verdin (2013) have shown that EM logging tools can have sensitivity to fractures filled with electrically enhanced proppant, although with a sensitivity limitation of 100 to 150m on the fracture extent away from the well bore.

This paper expands on the presentation of Hoversten et. al, 2014. We start with a simple economic model of a hypothetical reservoir as motivation for improvement in SRV estimates. This model, while hypothetical, is of an appropriate scale for many unconventional reservoirs. Its main purpose is to demonstrate the magnitude of the finantial impact measured over a reservoir's life span, due to improved SRV estimates, wherever they come from. With this motivation, we describe the proposed EM system and the numerical modelling required and test its sensitivity to hydraulic fractures at realistic depths and small sizes. The implicit assumption is that if a technique has high sensitivity to the existence and spatial distribution of a fracture or fracture zone then future work in inversion and integrated interpretation will be able to improve the ability to estimate SRV. It is hoped that the magnitude of the reward demonstrated by the financial model will stimulate the necessary additional research to incorporate EM into SRV estimation. We finish with demonstrations of EM responses over fractures, showing that they should be measurable and that they contain significant spatial information. Our results indicate that inversion of

such data should be able to provide valuable information on the spatial distribution of conductive proppant (either brine or electrically enhanced proppant).

A simple Economic Model

In order to appreciate the scale of the financial impact of improving the estimates of stimulated reservoir volume (SRV), we develop a simple, first order, financial model. The model is representative of large reservoirs in unconventional or tight formations. Its main purpose is to gauge the potential overall magnitude of the financial impact, without further conducting an in-depth financial analysis.

The parameters of the model are; 1) recoverable reserves in barrels (bbl.), with 42 US gallons per barrel, 2) the optimal number of wells to recover the reserves (assuming perfect knowledge of the drainage volume for each well), 3) well costs, 4) improvements in SRV estimates provided by geophysical surveys, 5) geophysical survey costs per well and per year, 6) discount rate for net present value (NPV) calculation, 7) drilling rate over the field's lifetime, 8) inflation rate, 9) capital expense after tax to before tax ratio (CapXATBT). The parameter values used for the example discussed here are given in Table 1.

The quantity *ideal_volume_per_well* is defined as the inverse of the number of wells to fully drain the field. The error in the SRV estimate is defined by equation (1):

$$SRV\_error = (Estimated\_SRV - ideal\_volume\_per\_well)/\, ideal\_volume\_per\_well \qquad (1)$$

We consider four possible improvements in the estimates of SRV, which are 2 %, 5 %, 10 %, and 20 %. We assume the average cost of geophysics to make the improvements in SRV is US$ 10,000 per well per year or US$ 1M per 100 wells per year. This reflects the view that the geophysics will not be conducted on every well but rather on areas of the field that have common geologic conditions. In order to determine if the geophysical cost is justified by the resultant savings, we do a net present value (NPV) calculation for the life of the field. The NPV is defined by equation (2):

$$NPV = \sum_{t=0}^{N} \frac{R_t}{(1+DCR)^t}, \qquad (2)$$

Where N is the number of years, R_t is the net cash flow at time t and DCR is the discount rate that represents the weighted average cost of raising capital to fund investments.

The discount rate is assumed to be 10%. We assume that there will be constant drilling of new wells for the first half of the field life (years of constant drilling in % = 50). After that, the number of wells drilled will decline linearly to zero at the end of the field life. The inflation rate (3%) and the capital expense after tax to before tax ratio (0.71) are assumed constant over the life of the field. The price of a barrel of oil is assumed to be $100.

In general, the maximum extent of the underestimated SRV will be lower than the maximum extent of the overestimated SRV, simply because the lower end is bounded by zero and the upper end is unbounded. This has led us to the choice of a simple asymmetric SRV probability density function (PDF) characterized by a maximum underestimate of -50% and a maximum overestimate of +200%. The PDF for the *SRV_error* given in (1) is displayed in Figure 1 in blue, with the *SRV_error* PDF for a 20% improvement shown in red. The % improvement causes the end points of the PDF to be decreased by the given % improvement.

The pseudo-code for the sampling part of the algorithm is given in Figure 2. The key is the random draws from the cumulative distribution function (CDF) that is associated with the defined *SRV_error* PDF's. Each random draw from the CDF defines one possible realization of an SRV estimate for a well given the assumed PDF for the errors. The draw is classified as either negative ($Estimated\_SRV$ is too small) or positive ($Estimated\_SRV$ is too big). For each year, there will be *number_wells_SRV_under*, and *number_wells_SRV_over* and the corresponding ideal volumes (*ideal_vol_SRV_under* and *ideal_vol_SRV_over*) for that number of wells in that year can be calculated. The estimated volumes (*under_estimated_vol* and *over_estimated_vol*) are calculated and the difference between the ideal and its estimate gives the redundant volume (*redundant_vol*) when *SRV_error* is negative and the missed volume (*missed_vol*) when the *SRV_error* is positive. When the *SRV_error* is negative, the number of wells that were not needed (*not_needed_wells*) are calculated and when the *SRV_error* is positive the wells that should have been drilled (*wells_should_have_drilled*) can be calculated.

Since drawing from the CDF provides one realization of the possible outcomes from the assumed random process, a large number of draws are needed to define the statistics of the model. In this example, 500 draws are used. This process is repeated for the new improved *SRV_error* PDF and the difference between the costs for the original and improved *SRV_error* are calculated. For the cases where the *SRV_error* is negative and too many wells are drilled, the P10, P50 (mean), and P90 quantiles of the *not_needed_wells* for both the original and improved *SRV_error* PDF's are calculated. P10, P50 and P90 are defined such that 10% of the estimates are less than or equal to the P10, 50% of the estimates are less than or equal to the P50 and 90% of the estimates are less than the P90. Equation 3 gives the

improvement in the number of wells that are not needed due to the reduction in the negative *SRV_error;* this is done for the P10, P50 and P90 values by year. Equations 3 and 4 represent vectors of length equal to the number of years of the field (24 in this example).

$$reduction\_in\_wells\_not\_needed = (original\_wells\_not\_needed - improved\_wells\_not\_needed) \quad (3)$$

The savings for the $reduction\_in\_wells\_not\_needed$ is given by Equation 3.

$$not\_needed\_well\_savings = (reduction\_in\_wells\_not\_needed * well\_cost * inflation\_factor) \quad (4)$$

The *inflation_factor* is calculated by compounding the inflation rate over the years of the field. The total geophysical costs (*TGC*) is the geophysical cost per well per year, accounting for inflation and the after-tax net present value (NPV_{AT}). The calculation of NPV_{AT} further involves the discount rate (*DCR*) and a capital-expense after-tax before-tax ratio ($CapXATBT$) as given by equation 5,

$$NPV_{AT} = \text{NPV}((not\_needed\_well\_savings * CapXATBT) - TGC \mid DCR) * (1+DCR)^{1/2} \quad (5)$$

The best representation of a yearly cash flow quantified by a single transaction per year is to assume that it occurs in the middle of the year. The $(1+DCR)^{1/2}$ multiplier thus adjusts equation 5 to this 'midpoint discounting', correcting for the fact that the NPV function assumes the cash flow occurred at the end of each year. The same process is used for the savings due to the improvement in the missed volume (*missed_vol*) when the *SRV_error* is positive.

Figure 3 shows the cost savings by year for $5 million wells and a 20% improvement in the *SRV_error*, using the PFD's shown in Figure 1. The savings are broken into savings from not having to drill so many wells in the case of *SRV_error* being negative and savings from accessing more reserves in the case of the *SRV_error* being positive.

The irregular nature of the curves comes from only using 500 samples, as the number of draws increases the curves smooth out. Over the first half of the field life (12 years), constant drilling results in ~ 277 wells per year and the inflation rate increases the value of the oil and well costs so the savings curves rise. After the drilling rate declines, the savings curves begin to decline toward zero. The P10 curves, where there is the minimal savings, illustrate that as the number of wells gets small, the random nature of the SRV estimates can produce situations where the SRV estimate from the improved PDF is worse than the SRV estimate from the original PDF producing a negative number. This highlights the reality that in small populations even doing the best geophysics can result in failure. The most obvious feature is that the savings from accessing more oil by reducing the overestimates of SRV far outweighs the savings from

drilling fewer wells when the SRV is underestimated. As well costs rise or oil prices fall, the two savings come closer to each other. The key result is the order of magnitude for the numbers produced by this model, in the case shown in Figure 3 the NPV_{AT} is 4.232 billion dollars over the life of the field for a 20% improvement in the SRV estimates.

Table 2 contains the NPV_{AT} values for $2 million and $5 million wells for a range of % improvements in the SRV error distributions for a $50 and $100 per barrel oil price. The NPV_{AT} values for the P10, P50 and P90 are shown. The sampling error estimated from multiple runs of 500 samples is 1.7%, meaning for any two simulations of 500 samples the final numbers can vary by 1.7%. The NPV_{AT} values for $2 million and $5 million wells are only slightly different because the bulk of the value comes from the recovered oil, which is the same in both cases. The fact that even a 5% improvement can result in a P50 savings over 1 billion dollars for $100/bbl. oil and 0.5 billion dollars for $50/bbl. oil, is the point of this exercise.

The model

During a typical hydro-frac operation, between 5,000 and 25,000 barrels of proppant-fluid slurry are injected into a tight formation. The proppant is typically sand of varying size whose purpose is to hold the created fractures open, once the pressure returns back to the natural formation pressure. Because an electromagnetic based technique relies on the electrical contrast between a target (the fracture) and the background for its sensitivity, we consider two ways of enhancing the contrast of the fracture and the background. The easiest and least expensive way is to increase the salinity (either NaCl or KCl) of the injected slurry. A second, more expensive and experimental approach is to enhance the electrical conductivity of the proppant itself, a case examined by Pardo and Torres-Verdin (2013).

The electrical conductivity of a solution is to first order a function of the salinity and temperature of the fluid. Assuming a geothermal gradient of 25C/km for the Permian Basin in West Texas (Ruppel *et al.* 2005) and an ambient air temperature of 10C the resistivity of NaCl solutions are taken from the Schlumberger Log Interpretation tables (Schlumberger 1997). These are plotted versus depth for NaCl concentrations of 10, 20, 50 and 100 thousand PPM in Figure 4. For fracs where normal sand is used, only the electrical conductivity of the fluid is considered since the slurry resistivity will be to first order the electrical resistivity of the brine since current will flow in the fluid.

When considering electrically enhanced proppant, the proppant and fluid must be treated as a mixture. During injection, typical proppant concentrations are on the order of 10-20% by volume. As the slurry moves into the created fracture, leak-off of the fluids into the formation concentrates the proppant resulting in a volume concentration as high as 50% within the fracture (Novotny, 1977). The electrical conductivity of the slurry with conductively enhanced proppant has been calculated using an equivalent media theory (Berryman & Hoversten, 2013). Figure 5 shows the slurry conductivity as a function of the fraction of proppant contained in the slurry. We have assumed a final proppant concentration of 40 % after leak-off, the 40% gives 526 S/m assuming a form of graphite coating on the sand, such as the coke-breeze material (Graphite, 2012) with an average conductivity of 3,333 S/m.

The size of the fracture zone in the model is based on a typical hydraulic-fracturing scenario in tight formations. The lateral and vertical extent is taken as 270 m x 90 m in the horizontal and vertical directions respectively. The lateral dimensions of the frac are purposely made asymmetric about the well, with the frac x extent from -120 m to +150 m. This is both realistic in that fracs rarely are symmetric about the well, but more importantly this allows quantification of the magnitude of the asymmetry in the observed fields as a measure of the EM system sensitivity to the frac geometry. The geometry of the fracture is idealized as a thin rectangular body; however the primary parameter that controls the EM system response is the conductivity-volume product of a fracture zone. This is true as long as the dimensions of the fracture zone are small relative to the distance from the source and receivers. The volume of the idealized fracture holds a realistic amount of conductive material that is on the low end of what is injected in practice, either brine or conductive proppant in fluid and thus is a suitable proxy for a single fracture or a fracture zone.

A 15% proppant concentration is assumed at injection and then a leak-off to 40% concentration prior to conducting the after-frac EM survey. A small injection of 5000 bbl. is modelled which results in a fracture volume of 1867 bbl. after leak-off. This equates to a 12.22mm by 270m by 90m fracture. Figure 6 shows the model for a fracture at 3km depth below the surface on a 1:1 scale. When considering a 100,000 PPM brine injection, we keep the volume equal to 1867 bbl., so that the conductive region is the same size for each frac conductivity. This means that the 100,000 PPM brine example is a very small volume and all but a few commercial jobs would be considerably larger, with a corresponding increase in the responses modelled. We consider the models presented here near the extreme in difficulty over the range of possible applications. Most frac jobs are larger than 5000 bbl., hence providing larger conductive targets, and many frac jobs are at shallower depths than the 3 km considered here. Shallower targets of the same size will have a larger EM response.

A vertical steel cased well is modelled with a 10 inch (0.254 m) outer diameter and 1 inch (2.54 cm) wall thickness. We assume the well casing is carbon steel with electrical conductivity of 5.0×10^6 S/m. One initial concern was the potential for corrosion (rust) on the outer casing and cement surrounding the casing to electrically isolate the casing from the earth. However, oil-field cement typically has resistivity in the range of 1 to 8 Ωm (Klein *et al.* 1993), which is more conductive than the background earth resistivity considered here. As to rust on the casings, measurements made by Marsala et al. (2014), where one source electrode is on the surface and a second electrode is inside a well, would not be possible if casing corrosion were limiting current flow into the earth. Intuitively this is reasonable since rust requires the presence of water and the exchange of ions, making the rust veneer a good conductor.

The application reported by Marsala et al. (2014) makes use of a downhole electrode to provide increased current density at depth and hence increase the response of the target fracs. While this is certainly a viable technology and may offer advantages due to increased deep current density in some circumstances, the potential negatives are the associated time and hence costs required to put sources downhole. A surface-based EM system that does not require well access has significant cost advantages as well as reduced resistance from field production administrators since taking wells offline is not required. To this end, we model a standard electric dipole source on the surface and simulate the measurement of surface electric fields. All results shown use a 50m grounded electric dipole source switching 30 A from on to off, with the fields shown as the decay of the electric field in the off time of the transmitter. The transmitter and receiver electrodes are located 0.0065m below the air-earth interface. The electric field noise measured by Hibbs (2015) at a frac site is reported as 1.0×10^{-11} V/Am^2 for a two second period, dual polarity waveform, stacked for 30 minutes (1800 samples). If a finer time resolution is desired stacking for 5 minutes would increase the noise level to by $\sqrt{1800/300}$ to 2.45×10^{-11} V/Am^2. We have used 3×10^{-10} V/Am^2 as a conservative number for the noise floor and no fields below this value are used in any of the percent difference calculations shown in subsequent figures.

Numerical Modelling

The system described above models the time-domain transient response of a grounded electric dipole surface based system using a finite difference (FD) based algorithm. The details of the algorithm are given in Commer & Newman (2004, 2006). We note that measurements can be made in the frequency domain with the use of synchronous detection as shown by Marsala *et al.*, (2014). However, among the time and frequency domain codes we have available, we have found that the explicit time-stepping code is more accurate for models with extremely high contrasts on the order of 10^8 to 10^9 in electrical

conductivity between steel wells and earth materials. The need to model the high contrasts will become evident in the next section.

A number of numerical tests were performed to assure the accuracy of the TDEM code used here; these are detailed in Commer, Hoversten and Um (2014) and include comparison to a 1D Sommerfeld integral code, a 3D solution for metallic spherical bodies and a 3D finite-element code. Several tests were run to optimize the vertical (z) grid spacing for these models. It was found that fine meshing in the vertical direction was not necessary. The transient results for meshes with Δz of 12.22 mm at the surface and increasing in size with depth were within a percent of results using a mesh with Δz of 20m at the surface increasing by 8% downward. All results shown here have the Δz 20m at the surface increasing by 8% for each cell downwards until the frac zone is reached. The frac zone has two z cells of 45m each for the total vertical extent of 90m. The z dimensions start at 30m in the air and increase by 50% for each cell upwards. The boundaries of the meshes are at 400km in all dimensions.

Our initial model tests used material averaging of the conductivities for steel wells and the surrounding earth into model cells of 0.5 m in the x and y directions, using the material averaging scheme presented in Commer & Newman (2006). While this approach has proven effective for modeling earth conductivity contrasts on the order of 10^3 or less, it breaks down when we try to average steel casings into large (relative to the size of the conductive object) FD cells. Figure 7 shows the transient electric fields measured at x, y, z coordinates of (-150, 10, 0) from a 50m 30A dipole source centered on x, y, z of (-200, 0, 0). The well is centered at the origin and the frac is shown in Figure 6 in a 100 Ωm halfspace. The frac conductivity is 526 S/m. The response of the casing with and without the frac are plotted for the upscaled response (x and y cells are 0.5m) and the response calculated from the fine FD mesh using 12.22 mm cells in the x and y directions. The 12.22 mm meshing in the casing's vicinity allows the casing wall to be represented by two cells., A horizontal close up view of this mesh region is shown in Figure 8.

Figure 7 demonstrates that while the upscaled results are similar in terms of the shape introduced by the frac, the magnitude of the responses are different. Figure 9 shows a significant difference in the percent differences between the casing only and casing + frac models for the upscaled and fine FD solutions. The percent difference is defined in equation 6,

$$\%difference = \left(\frac{(Frac + Casing) - Casing\ only}{Casing\ only}\right) * 100. \quad (6)$$

The upscaled response underestimates the anomaly caused by the frac in the presence of casing by 35% in Ex and Ey (the Ey % difference is calculated at the last time where both Ey values are above the $3x10^{-10}$

V/m assumed noise floor). The problems encountered in upscaling by arithmetic and harmonic means of the conductivity has been noted by Caudillo-Mata *et al*. (2014) and while they offer an algorithm to remediate the situations, they note that upscaling is highly problem- specific and always an approximation. Therefore we have chosen to use the fine FD meshing to ensure the most accurate results possible. The use of the fine meshes comes at considerable compute expense. While the upscaled models run in 25 minutes using 252 Sandy-bridge cores, the fine mesh models run in 28.5 hours using the same resources.

The effects of steel casing

The geophysical literature contains many papers on the effects of steel infrastructure, most commonly well casings, on EM measurements. In almost all cases, the effects of the steel casing are considered as a noise source. The exceptions have been where the casings are considered as long vertical electrodes for DC resistivity measurements (i.e., Rocroi and Koulikov, 1985; Daily *et al.*, 1990). Takacs (1998) specifically notes that for a frequency domain system, "Application of these steel casings as an antenna can increase the current density in deep structures compared to the case of surface source." Yang *et al.* (2009) study directly injecting current into steel casing for surface and cross-well measurements. The work presented here demonstrates that steel casing acts to channel significant current down into deep small conductors (electrically enhanced fractures) from grounded electric dipole sources in the vicinity of, but not contacting, wells. This allows the EM response from such targets to be significantly enhanced compared to the response when the casing is not considered.

Figure 10 shows the radial E field at x=10, y=10m with the well at (0, 0) in the canonical model with a 10 Ωm background when a 50m x-directed electric dipole with 30 A straddles the well with end point (x,y,z) coordinates of (-25, 0, 0) and (+25, 0, 0). The field is radial and the receiver is offset to simulate the fact that measurements could not be made at the well pad. The dashed curve pair is calculated from the model without the brine-filled steel casing. The dashed black curve is the 10 Ωm background step-off responses, and the red triangles are the response with the frac included. The solid curves stem from the model that contains the cased wellbore, where black and red curves correspond to no-fracture (halfspace and casing) and fracture case, respectively. Including the casing in the simulation completely changes the response and provides a significant difference in the measured E field when the frac is introduced. Figure 11 shows the percent differences caused by the presence of the frac at 526 S/m in the 10 Ωm background when the casing is included in the calculations for four E field components, Ex, Ey, Ez, and Er. The maximum response from the frac is ~ 16 % at 0.55 seconds after turn off in the Ey component. All the

fields are well above the assumed instrument noise floor of $3.0x10^{-10}$ V/m in the time window of maximum response.

In order to understand the large positive effects of the casing on the response due to the fracture, the currents in the model with a 10 Ωm background are plotted with and without the casing in Figures 12 and 13 for 0.001 and 0.1 seconds after transmitter turn off. Comparing the current distributions with and without the casing shows that the casing acts to collect current in the near surface and channels it down into the frac. The zone where net current flows into the casing is ~ the upper 200m at 0.001 seconds and ~ the upper 1300m at 0.1 seconds. At 0.001 seconds after turn off the maximum horizontal current in the casing connected to the frac is 330 times greater than without the casing. At 0.1 seconds after turn off the ratio of casing-connected to no-casing horizontal current increases to 750. The large boost in the frac current when the casing is coupled to the frac explains why the response at the surface is significantly enhanced compared to when the casing is not modeled. It should be noted that these results indicate that any electromagnetic modeling using electric dipole sources for reservoir monitoring applications must include the well casings in the calculations.

Surface E field responses

Two background resistivities are considered here. A 10 Ωm background is representative of many shale plays, for example in many locations where the Niobrara shale of the western United States is the target, 10 Ωm is a good approximation to the overburden and shale resistivity. A 100 Ωm background is representative of many plays in carbonate or carbonate-derived formations. The Permian Basin in the United States actually has background resistivities higher than 100 Ωm. The response of the canonical frac (Figure 6) in backgrounds with resistivity higher than 100 Ωm will be even larger than shown here.

In order to define a minimum percent difference that would be discernable in the field we use the measured data shown in Figure 5 of Hibbs 2015. The difference between the before and after frac electric fields in the on-time are clearly visible with a mean % difference of 4.1% with a standard deviation of 0.7%. These measurements can be improved to further reduce the noise levels with additional processing such as magnetotelluric signal prediction and removal which is standard in EM signal processing. From the data set collected by Hibbs (2015) we conclude that a 2% difference can be distinguished in high quality field data. The reader can determine a percent difference they feel comfortable with when interpreting the percent differences we calculate, fortunately most of the responses computed here are well above a 2% threshold.

A number of source-receiver configurations were considered. A single source and a number of receivers laid out over the frac are shown in Commer *et al.* (2015). However, the best array to demonstrate the spatial resolution and maximum sensitivities to the frac was found to be a profile of sources and receivers that could be sorted into constant-offset so that the data can be plotted as source-receiver midpoint versus time for a given offset.

Figure 14 shows such time-pseudo sections of the radial electric field where thirteen source-receiver pairs are used. Figure 14 a) show the percent difference when the X separation between source center and receiver is 0m, Figure 14 b) is for a +50 m X separation. The profiles are run over the frac shown in Figure 6 in a 10 Ωm background. The 50m transmitters are centered every 50m from -300m to +300m at y=0m. The line of receivers is run at y = +10m to avoid the well pad. The lateral extent of the frac is shown by the vertical white lines. The radial electric field is smoothly varying as the array passes the well and produces the largest percent difference, with a maximum of 11.1% for the 0 X separation and 15.4% for the +50m offset in this example. The X component of the electric field for comparison has a maximum percent difference of 9.4%. The asymmetry in the frac extent about the well is seen in the asymmetry of the percent difference. The maximum asymmetry in the radial electric field % difference is -8.4% on the long side of the frac for the 50m source-receiver offset and only 0.07% for the 0 X separation. Percent differences for source-receiver X separations of 0, 10, 25, 50, 75, and 100m for all the models considered with the results of the maximum percent difference and the maximum asymmetry in the responses are given in Table 3.

The character of the spatial and temporal distribution of the percent differences as a function of the source-receiver offset changes from small to large offsets, with the zero-offset responses being nearly symmetric and the asymmetry in the percent difference increasing with offset.

Figure 15 shows the before and after percent differences for the same source-receiver configuration and frac when the background is 100 Ωm. The reduced attenuation in the 100 Ωm background compared to the 10 Ωm background has increased the percent difference to a maximum of 213% when the X direction source-receiver separation is 50m. When the X direction source-receiver separation is 0m the maximum percent difference is reduced to 172%. The maximum response comes at an earlier time compared to the 10 Ωm response, reflecting the increase in the phase velocity in the more resistive material. The asymmetry in the percent difference is proportionally increased to a maximum of --95% and -14% on the long side of the frac for X direction offsets of +50m and 0m respectively.These models show large

responses and spatial sensitivity to the dimensions of the frac, as seen in the asymmetrical responses to an asymmetrical frac; however they make use of a conductively enhanced proppant. While such proppant is under development by contractors, it will no doubt be more expensive than brine solutions. The canonical model was run in a 100 Ωm background with a 100,000 PPM brine providing a frac conductivity of 30.5 S/m compared to the 526 S/m achieved with the conductive proppant. Figure 16 show the percent differences for comparison between 526 S/m and 30.5 S/m for the frac. The same thirteen transmitter locations with X direction separations of 0 and +50m between source midpoints and receivers are used as before. The brine filled frac produces a maximum 23.6 and 20.3 percent difference for +50 and 0 X direction separations respectively, well above the 2% limit indicated from field data (Hibbs, 2015), with greater than a 5% asymmetry in the spatial response for source-receiver separations of 50m and more.

Figure 17 shows the before and after percent differences for the thirteen source array across the 10 Ωm model with 100,000 PPM brine (frac at 30.5 S/m). Now the maximum percent difference is reduced to 1.7 and 2.3 percent for source-receiver separations of 0 and 50m respectively with the maximum asymmetry in the response is -1.3% at +50m separation on the long side of the frac. This probably represents the limits of detection for small 1875 bbl. frac's with realistic brine concentrations at 3km depth. However, since 1875 bbl. is a relatively small frac volume, larger 100,000 PPM brine fracs at this depth are likely to produce measurable E field responses.

Discussion

We present what we consider a feasibility study to show order of magnitudes and to stimulate further work. The models are simple, in particular the hydro-frac is represented as a single perfectly rectangular crack whereas in reality there will be some domain with multi fractures dissipating the conductive material (brine or proppant) over a larger volume. We have not considered the leak-off of injection fluid into the surrounding rock. In the case of the conductive proppant models we only model 1875 bbl. of 40% proppant in the idealized fracture from a total injection of 5000 bbl. The additional 3125 bbl. or fluid that leaks off may increase or decrease the surrounding rock conductivity depending on the in-situ fluid conductivities. Consideration of the total effect will require hydraulic modeling of the flow in and around the fracture zone.

Proppant does not uniformly fill the fracture(s); rather, its concentration is higher near the well and at the bottom of any fractures. The effects of proppant and brine distributions within the fracture network need to be modeled. The results for conductive brine are less likely to be significantly different from real applications because the brine will be able to penetrate without the effects of proppant dropout. The

overburden is a simplified halfspace, while in a 3D anisotropic conductivity structure currents will be distorted and surface patters of the response may not center on the frac. All of these complications can and should be modeled. We have shown the time-pseudo sections for the Ex (in-line with the transmitter fields) which show significant responses. However, the models show that the null-coupled Ey field and the Ez fields have even larger responses. While Ez is difficult to measure, Ey is not and offers the potential for measurable signals from even lower contrast or deeper targets. Notwithstanding the simplifications used here, we believe these results demonstrate that measurable signals from hydro-fracs of an economic scale should be observable with modern EM systems. In addition, the spatial variability of the responses offer hope that inversion of surface EM data can provide some constraints on the location of fluid and proppant. We have done some preliminary examinations with 3D pixilated inversions and found them to provide very low resolution. New hybrid schemes that parameterize the fracture(s) as sheets or use level-sets to describe thin discrete conductors embedded in a 3D pixilated background are under examination and development. We hope to report on the applications of these new inversion techniques in more complex geologic setting in the near future.

Conclusions

A financial analysis of the benefits of even small improvements of the error in SRV estimates shows that for fields with 1 billion bbl. recoverable reserves even a very modest improvement of 5% in the SRV provides over 1 billion dollars net present value over a 24 year field life. We believe that current SRV errors are large and that there is significant room for all sorts of geophysical technology to make significant improvements and hence have very large financial impacts.

The effects of steel cased wells on electromagnetic systems are most commonly considered a problem rather than the benefit we have shown it to be. Modeling the casing is a difficult numerical problem due to the extreme spatial scale and conductivity differences that must be represented to capture the well, the fractures, the EM system, and the earth. However, this work demonstrates that the continuing development of algorithms and increased compute power now make forward modeling of casing possible. Work is underway to increase the computational efficiency so that inverse problems will shortly be feasible.

This work shows that fracs from relatively small injections (5000 bbl.) using either conductively enhanced proppant or high salinity brines at depth up to 3km can be detected in electric field measurements at the surface using conventional electromagnetic exploration systems. This renders the drilling of additional monitoring wells unnecessary which is further expected to impact the savings for the

$reduction\_in\_wells\_not\_needed$, given by Equation 3. The spatial asymmetry seen in the percent differences for before and after measurements for asymmetric frac geometries indicates that there is good spatial information in the surface electric fields. These results are very encouraging for the development of inversion algorithms which can delineate the extent of created fractures and thus potentially provide improvement in the SRV estimates.

Significant advancements in the improvement of SRV estimates will most likely come from the integration of electrical and seismic data coupled with flow simulation. Several groups are currently working on a variety of joint geophysical and flow forward and inverse modeling to address this problem. We believe that electrical data will add to the mix over the next few years.

References

Berryman, J.G. and Hoversten, G.M. 2013. Modeling electrical conductivity for earth media with macroscopic fluid filled fractures. Geophysical Prospecting, **61**, 471-493.

Caudillo-Mata, L.A., Haber, E., Heagy, L.J., and Oldenburg, D.W. 2014. Numerical Upscaling of Electrical Conductivity: A problem specific approach to generate coarse-scale models. SEG Denver 2014 Annual Meeting Expanded Abstracts, p 680-684.

Commer, M., and Newman, G.A. 2004. A parallel finite-difference approach for 3D transient electromagnetic modelling with galvanic sources. Geophysics, **69**, 1192-1202.

Commer M. and Newman, G.A. 2006. An accelerated time domain finite difference simulation scheme for three-dimensional transient electromagnetic modelling using geometric multigrid concepts. Radio Science, **41**, RS3007, doi:10.1029/2005RS003413.

Commer, M., Hoversten, G.M., Um, E.S. 2014. Transient-electromagnetic modelling of steel infrastructure. Geophysics, Accepted for publication.

Daily, W.D., Owen, E., and LaBrecque, D.J. 1990. Cross-borehole electrical resistivity tomography. SEG Technical Program Expanded Abstracts 1990, 573-574.

Graphite, 2012, Coke breeze backfills for cathodic protection, www.farwestcorrosion.com/coke-breeze-backfills-by-asbury-graphite.html.

Hibbs, A.D., 2015, Evaluation of Deep Subsurface Resistivity Imaging for Hydrofracture Monitoring. US Department of Energy, National Energy Technology Laboratory, Fifth Quarterly Progress Report, Project Number: DE-FE0013902.

Hoversten, G.M., Commer, M., Haber, E., Schwarzbach, C. 2014. Hydro-frac Monitoring Using Ground Time-domain EM. 76th EAGE Conference and Exhibition – WS09-C08, DOI: 10.3997/2214-4609.20140565 .

Klein, J.D., Martin, P.R., and Miller, A.E. 1993. Cement Resistivity and Implications for Measurement of Formation resistivity Through Casing. SPE, 26453, 365-380.

Marsala, A.F., Hibbs, A.D., Morrison, H.F. 2014. Borehole Casing Sources for Electromagnetic Imaging of Deep Formations. SPE Annual Technical Conference and Exhibition, Oct 27-29, Paper # 170845. Amsterdam, Netherlands.

Novotny E.J. 1977. Proppant transport. SPE paper 6813 presented at the 52nd Annual Fall Technical Conference and Exhibition of the Society of Petroleum Engineers of AIME held in Denver, Colorado, October 9-12, 1977.

Pardo, D., Torres-Verdin, C. 2013. Sensitivity analysis for the appraisal of hydrofractures in horizontal wells with borehole resistivity measurements. Geophysics, **78**, D209-D222.

Rocroi, J.P. and Koulikov, A.V. 1985. The use of vertical line sources in Electrical Prospecting for Hydrocarbon. Geophysical Prospecting, **33**, 138-152.

Ruppel, S.C., Jones, R.H., Breton, C.L., Kane, J.A. 2005. Preparation of Maps Depicting Geothermal Gradient and Precambrian Structure in the Permian Basin. USGS Order no. 04CRSA0834 and requisition no. 04CRPR01474.

Schlumberger Interpretation Charts, 1997. SMP-7006.

Takacs, E. 1998. A Nonconventional geoelectric Method Using EM Field generated by Steel-casing excitation. SEG Technical Program Expanded Abstracts 1998, 452-455

Yang, W., Torres-Verdin, C., Hou, J., Zhang, Z. 2009. 1D subsurface electromagnetic fields excited by energized steel casing. Geophysics, **74**, E159-E180.

Model Parameters	Values
Field Life (yr)	24
Recoverable (MM bbl)	1000
Price of 1 barrel of Oil ($US)	100
Optimal # wells	5000
% years of constant drilling (%)	50
Discount Rate for NPV (%)	10
Annual Inflation rate (%)	3
Corporate Tax Rate (%)	37
Average Geophysical cost per well ($MM)	0.01
Well cost ($MM)	2, 5
Improvement in SRV (%)	2,5,10,20
Low End SRV error (%)	-50
High End SRV error (%)	200

Table 1: Parameters for financial model.

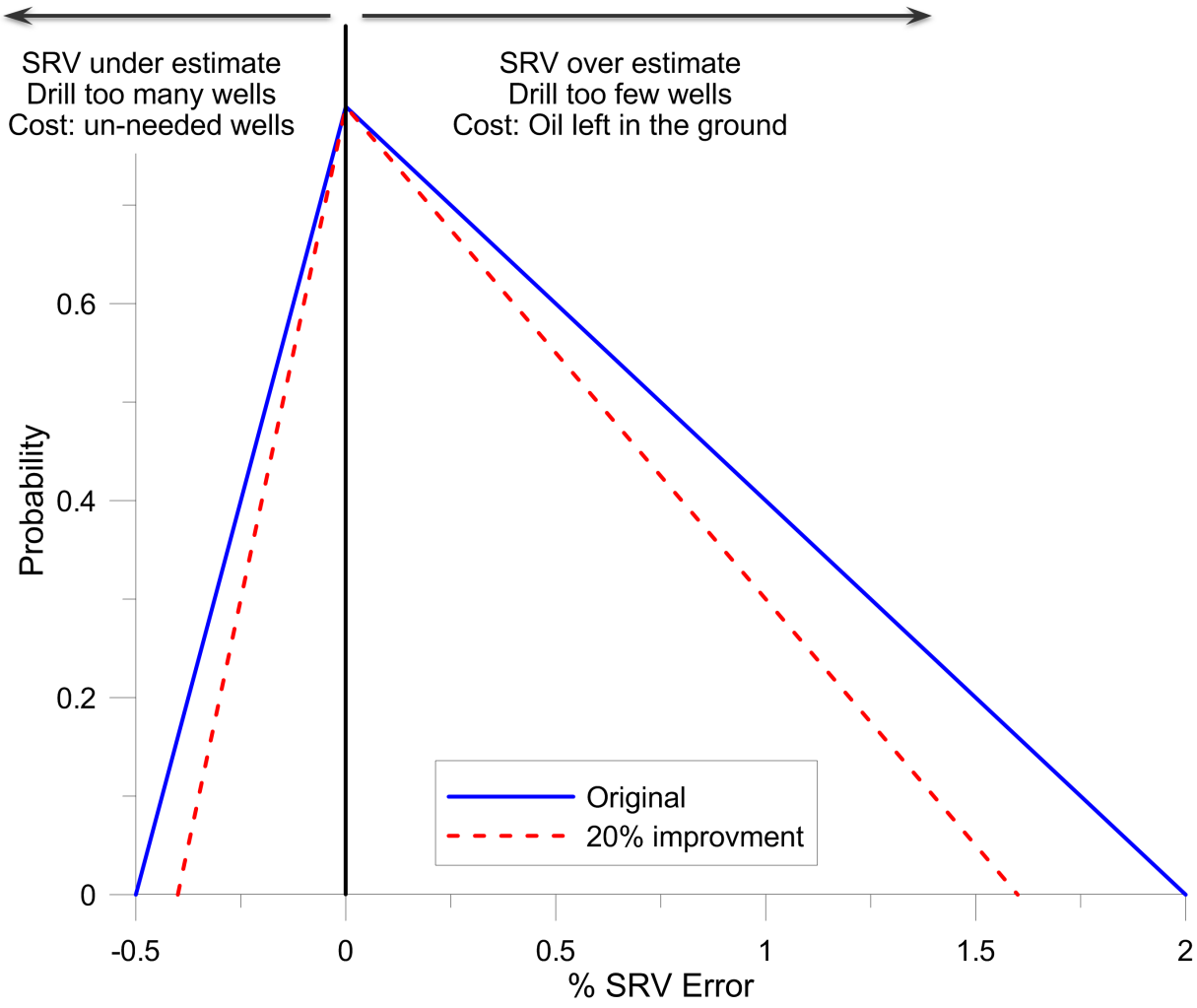

Figure 1. The initial assumed SRV error PDF is the solid blue line with the 20% improved SRV error PDF as the dashed red line.

```
% Definition
% SRV_error = (Estimated_SRV - Ideal_volume_per_well)Ideal_volume_per_well;
%
for k = 1 : number_of_draws_from_distribution
  for i=1 : total_years_in_field_life
    for j = 1 : number_of_wells_per_year(i)
      %
      % randomly draw from the cumulative distribution
      %
      SRV_error(j) = draw from SRV_error Cumulative Distribution
    end
    %
    % Est_SRV is a VECTOR of length number_of_wells_per_year(i)
    %
    Est_SRV = (SRV_error * I deal_volume_per_well) + Ideal_volume_per_well;
    %
    % seperate based on sign of SRV_error
    %
    it = SRV_error < 0;      % list the indexes where SRV_error is < 0
                             % ~it is list of indexes where SRV_error is >= 0
    %
    % for SRV_error < 0
    %
    number_wells_SRV_under(i,k) = sum(it);
    ideal_vol_SRV_under(i,k)    = number_wells_SRV_under(i,k) * Ideal_volume_per_well;
    under_estimated_vol(i,k)    = sum(abs(Est_SRV(it)));
    redundant_vol(i,k)          = ideal_vol_SRV_under(i,k) - under_estimated_vol(i,k);
    not_needed_wells(i,k)       = redundant_vol(i,k) / Ideal_volume_per_well;
    %
    % for SRV_error > 0
    %
    number_wells_SRV_over(i,k)  = sum(~it);
    ideal_vol_SRV_over(i,k)     = number_wells_SRV_over(i) * Ideal_volume_per_well;
    over_estimated_vol(i,k)     = sum(abs(Est_SRV(~it)));
    missed_vol(i,k)             = over_estimated_vol(i,k) - ideal_vol_SRV_over(i,k);
    wells_should_have_drilled(i,k) = missed_vol(i,k) / Ideal_volume_per_well;
  end
end
```

Figure 2. Pseudo-code for financial model

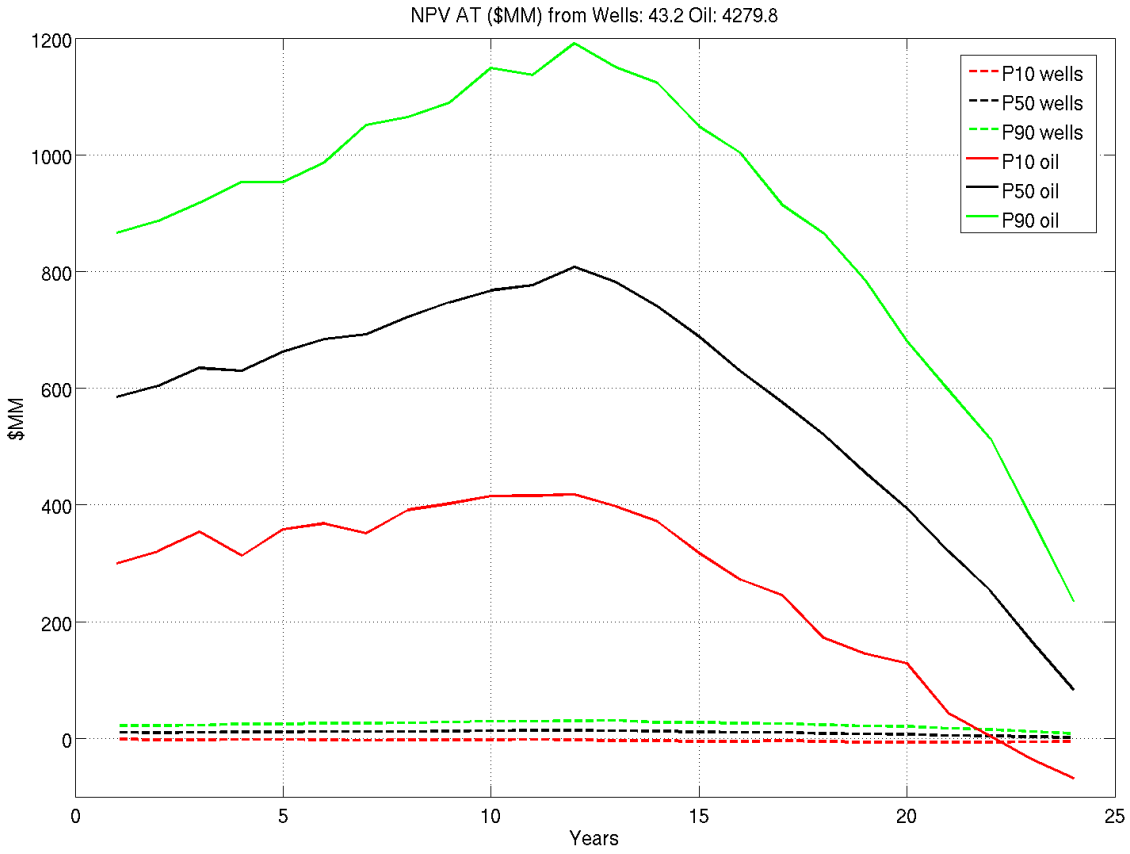

Figure 3. Calculated savings by year from the original SRV PDF and the 20% improvement in SRV error PDF shown in Figure 1. P10, P50 and P90 quantiles are shown as red, black and green curves respectively. Wells are assumed to cost $5 million. The price of oil is assume to b 100$/bbl. Solid curves are the savings from improved oil recovery by reducing the overestimates of the SRV per well and the dashed curves are the savings from elimination of redundant wells by improving the underestimation of the SRV per well. The savings from oil recovery clearly dominates given the assumed parameters. The P50 total after tax net present value (NPV) of the geophysics used to reduce SRV prediction error by 20% is $4.323 billion ($10^9$).

After Tax NPV in $MMM ($10^{9}$)						
% improvement	2 $MM well cost @ $100/bbl			5 $MM well cost @ $100/bbl		
	P10	P50	P90	P10	P50	P90
2	-1.92	0.383	2.75	-2.076	0.392	2.783
5	-1.25	1.075	3.37	-1.25	1.086	3.43
10	-0.11	2.16	4.39	-0.182	2.119	4.44
20	2.16	4.322	6.42	2.1	4.323	6.54

% improvement	2 $MM well cost @ $50/bbl			5 $MM well cost @ $50/bbl		
	P10	P50	P90	P10	P50	P90
2	-0.996	0.199	1.383	-1.034	0.196	1.447
5	-0.65	0.524	1.693	-0.707	0.534	1.762
10	-0.084	1.066	2.207	-0.0128	1.078	2.275
20	1.064	2.143	3.228	1.043	2.193	3.337

Table 2. After Tax net present value (NPV_{AT}) for variable % improvement in the SRV error PDF for a 1 billion bbl. field with 25 year field life. The ideal number of wells to drain the field assumed to be 5000. Assumed geophysics costs is $1 million per 100 wells per year. Original SRV error PDF defined as linear ramps from -50 to 0 to +200 percent error (blue curve in Figure 1). Discount Rate for NPV calculation assumed to be 10% with an annual inflation rate of 3% and a capital expense after tax to before tax ratio of 0.71. Price of a barrel of oil is assumed to be $100 for the upper table and $50 for the lower table.

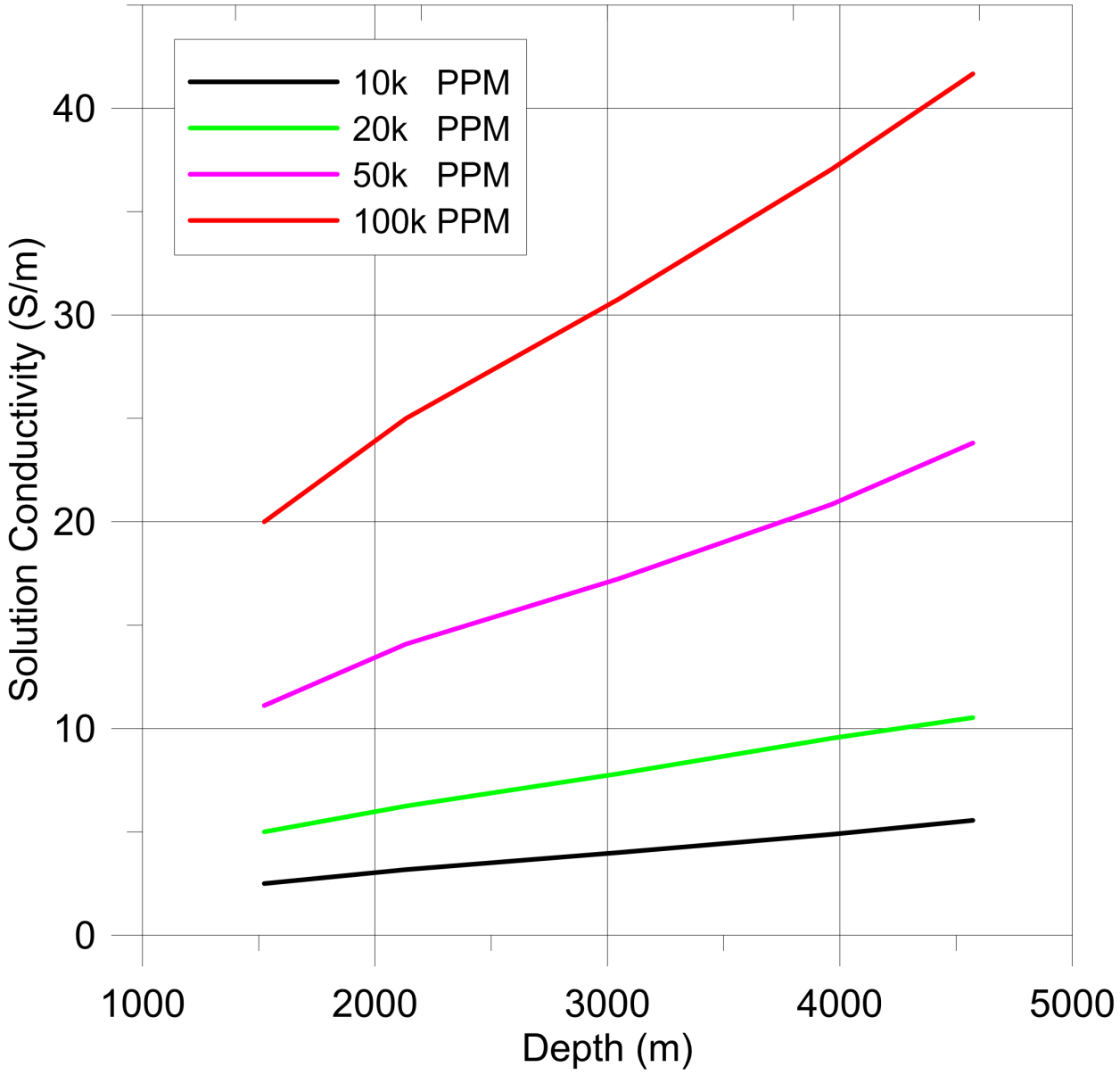

Figure 4. Solution conductivity as a function of depth (temperature is converted to depth using the geothermal gradient) for NaCl concentrations of 10,000, 20,000, 50,000, and 100,000 PPM. Calculations are done assuming the Permian Basin geothermal gradient of 25C/km and an ambient air temperature of 10C.

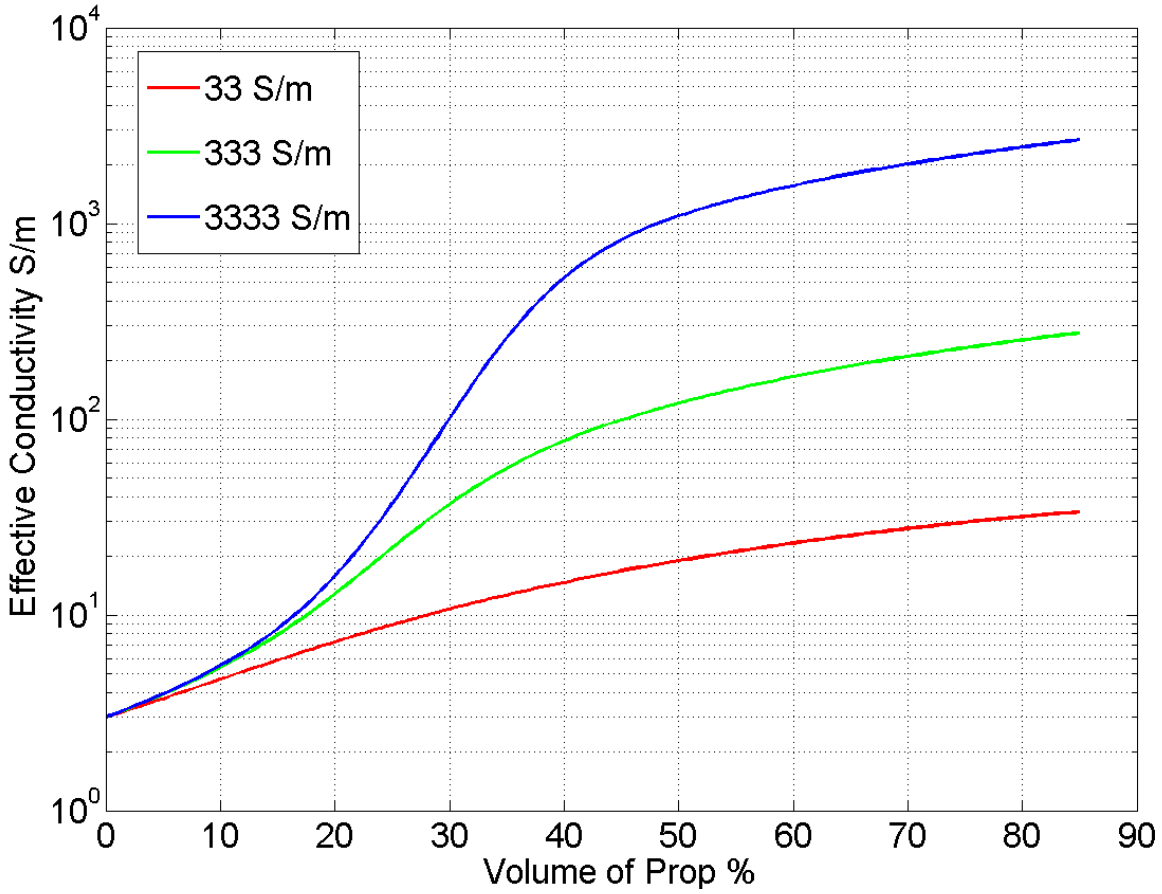

Figure 5. Effective conductivity of a brine based slurry containing conductively enhanced proppant as a function of proppant concentration. The mixing model (Berryman & Hoversten 2013) is used assuming spherical grains. Taking the conductivity of coke-breeze coated sand as 3,333 S/m would result in a slurry conductivity of 526 S/m at a 40% sand concentration.

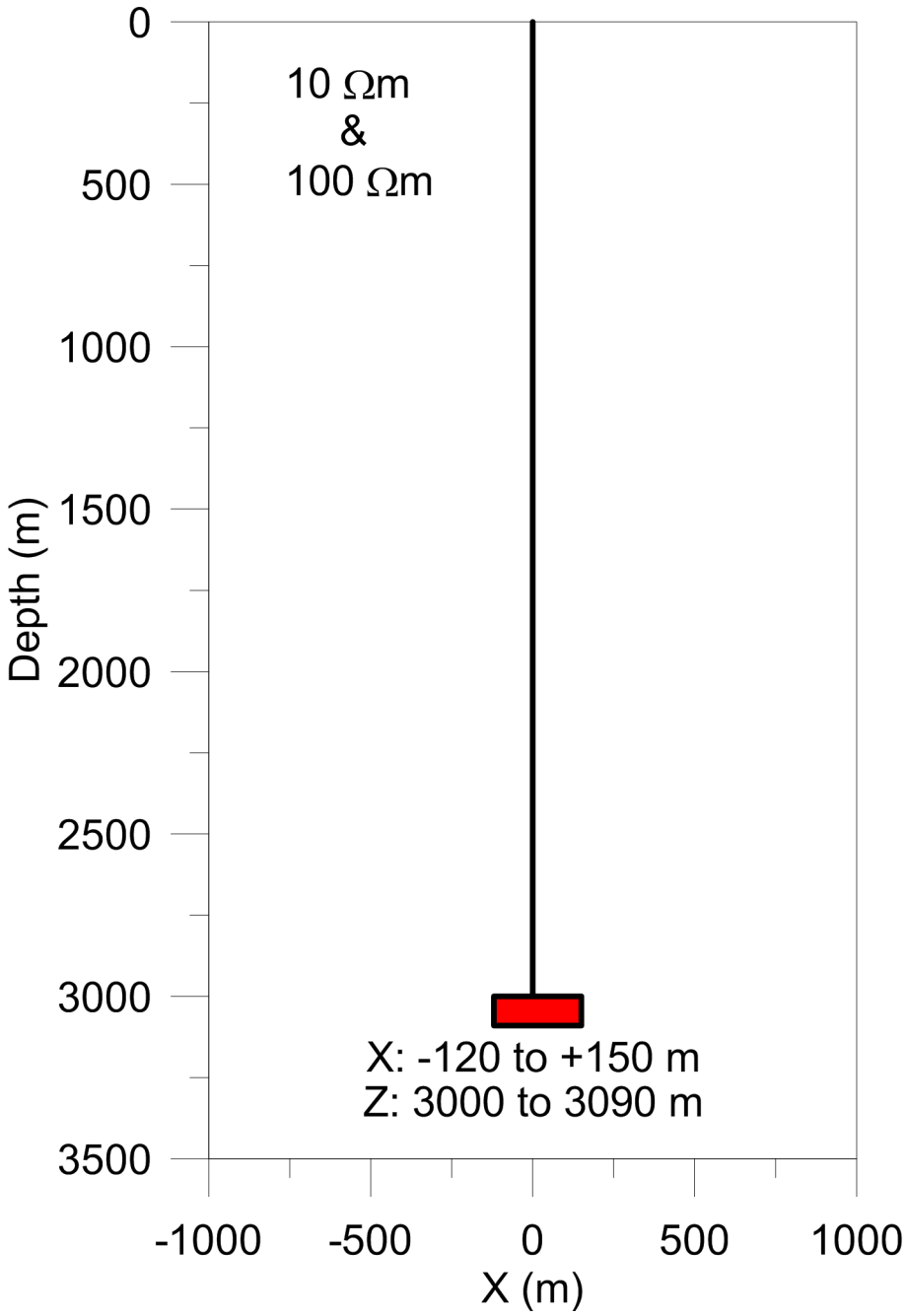

Figure 6. The canonical model for 5000 bbl. injected at 15% proppant leaving 1867 bbl after leak off to 40% conductive proppant concentration. The red box is the 12.22mm thick frac with x extent from -120 to +150m and vertical extent from 3000 to 3090m. The top of the frac is at 3km depth. The Vertical/Horizontal scale is 1:1.

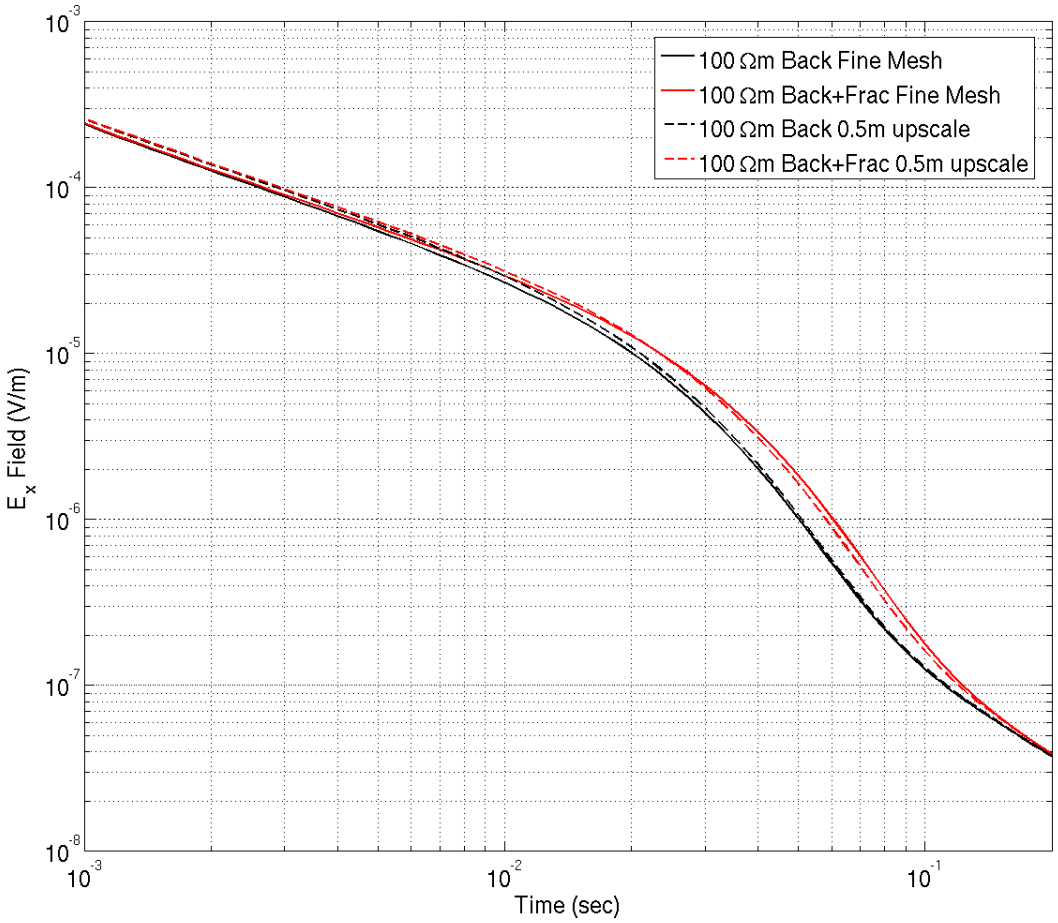

Figure 7. Transient Ex, in-line with the transmitter dipole. The frac shown in Figure 6 is embedded in a 100 Ωm halfspace. The conductivity of the frac is 526 S/m. The 50m long, 30 Amp dipole is centred on x = -200m, y = 0m with the receiver at x = -150m, y = 10m. This is the same source-receiver offset used in the profile responses shown in Figures 14-18. The solid black line is the response from a fine FD mesh with 12.22mm cells in the x and y directions to capture the casing response. The solid red line is the fine FD mesh with casing and frac present. The dashed black line is the upscaled response using 0.5m cells in the x and y directions of the casing only and the dashed red line is the upscaled response for casing and frac.

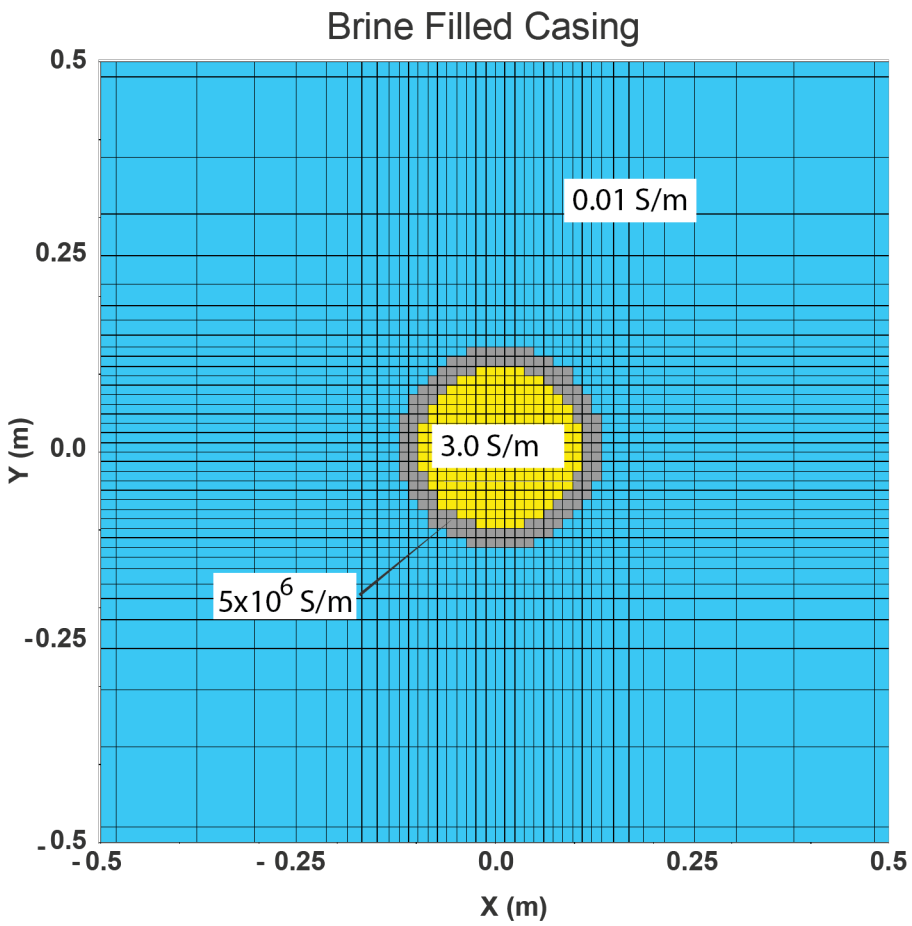

Figure 8. Horizontal X-Y section around the steel well casing in the fine FD mesh used to calculate the responses in this paper. The smallest cell dimensions are 12.22 mm. The mesh is uniform in x and y around the casing and then grows by a factor of 1.2 per cell to the outer boundaries. Vertical cell size gradually grows from 20 m from the air-earth interface to 50m at a depth of 3200m.

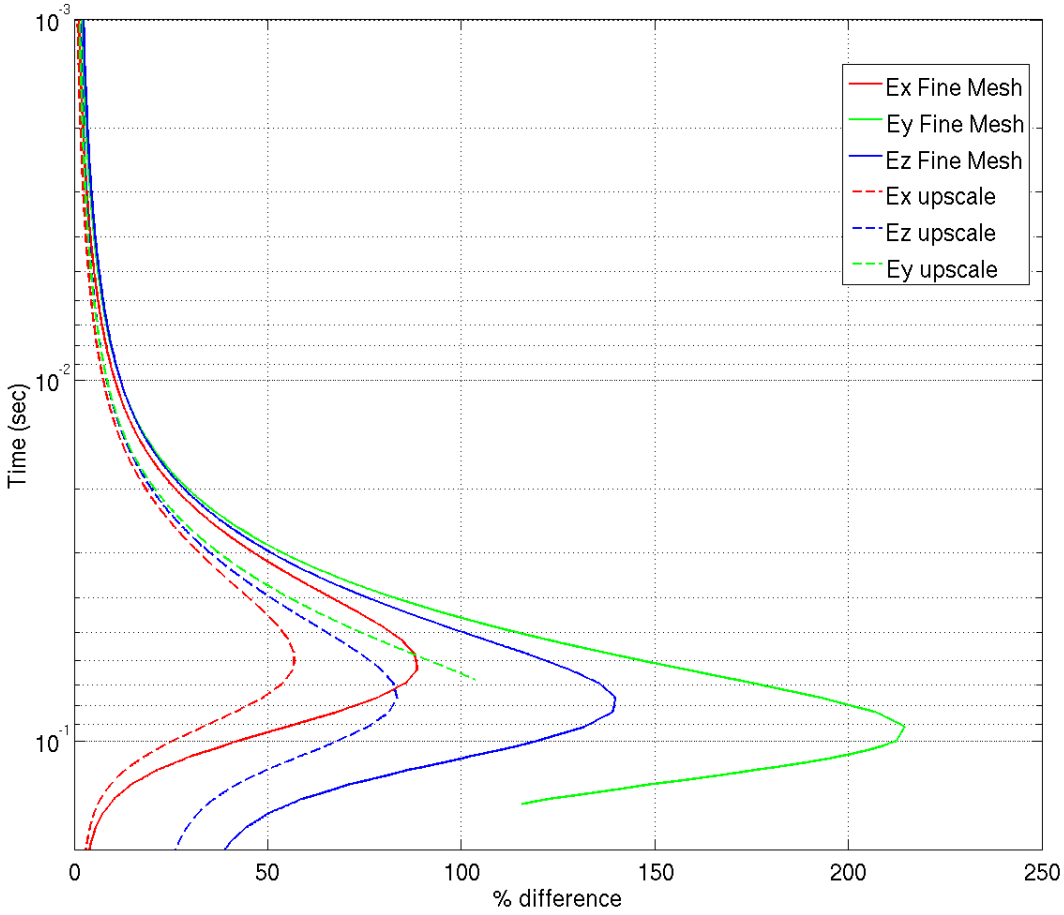

Figure 9. Percent difference between the casing-only and casing-plus-frac models shown in Figure 7. The solid lines are from the fine mesh (12.22mm cells in x and y) and dashed lines are from the up scaled mesh (0.5m cells in x and y). Ex fields are red, Ey fields are green and Ez fields are blue. The frac shown in Figure 6 is embedded in a 100 Ωm halfspace. The conductivity of the frac is 526 S/m. The 50m long, 30 Amp dipole is centred on x = -200m, y = 0m with the receiver at x = -150m, y = 10m. Curves stop where the field values drop below 3.0×10^{-10} V/m.

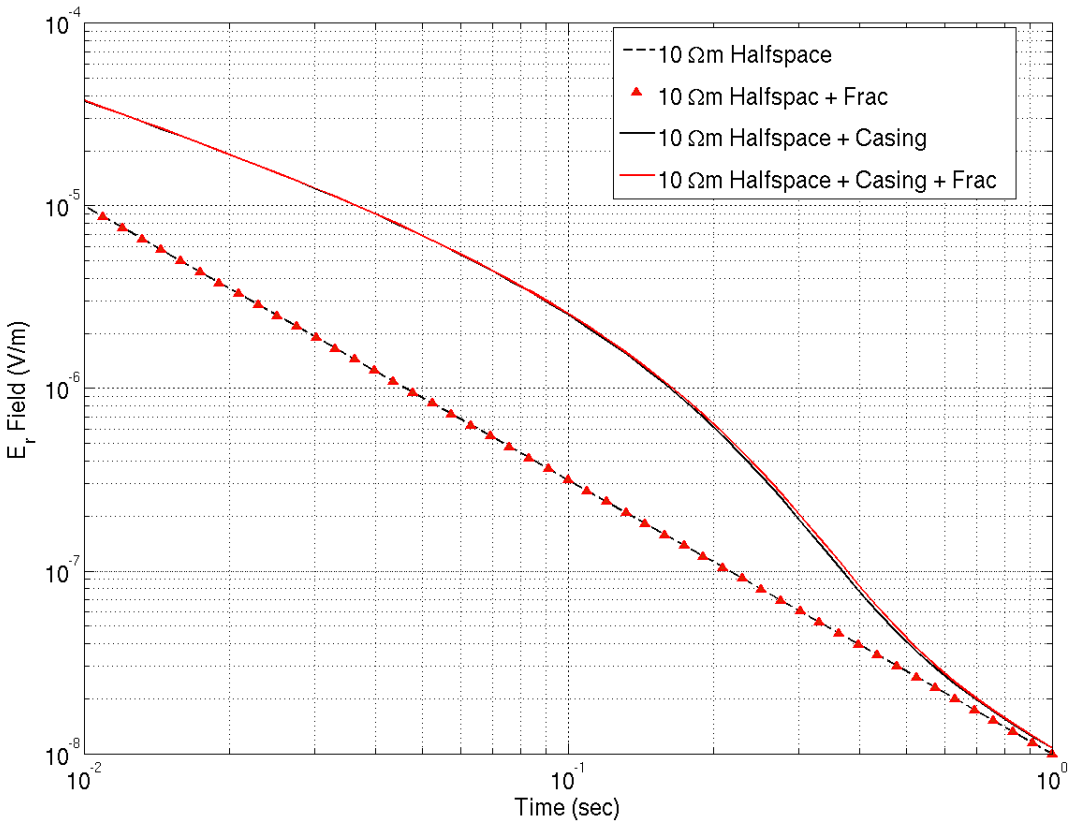

Figure 10. Step off E in the radial direction between the source mid-point and the receiver point for a 50m 30 A dipole with (x, y, z) end points at coordinates (-25, 0, 0) and (+25, 0, 0). The receiver is offset from the well at x=10m and y=10m. The canonical model frac is shown in Figure 6 with the coke-breeze coated sand resulting in a fracture conductivity of 526 S/m. The dashed black line is 10 Ωm halfspace response. The red triangles are the 10 Ωm halfspace with the frac. The solid black line is the 10 Ωm halfspace with the well casing modelled. The solid red line is the 10 Ωm halfspace with the casing and frac modelled.

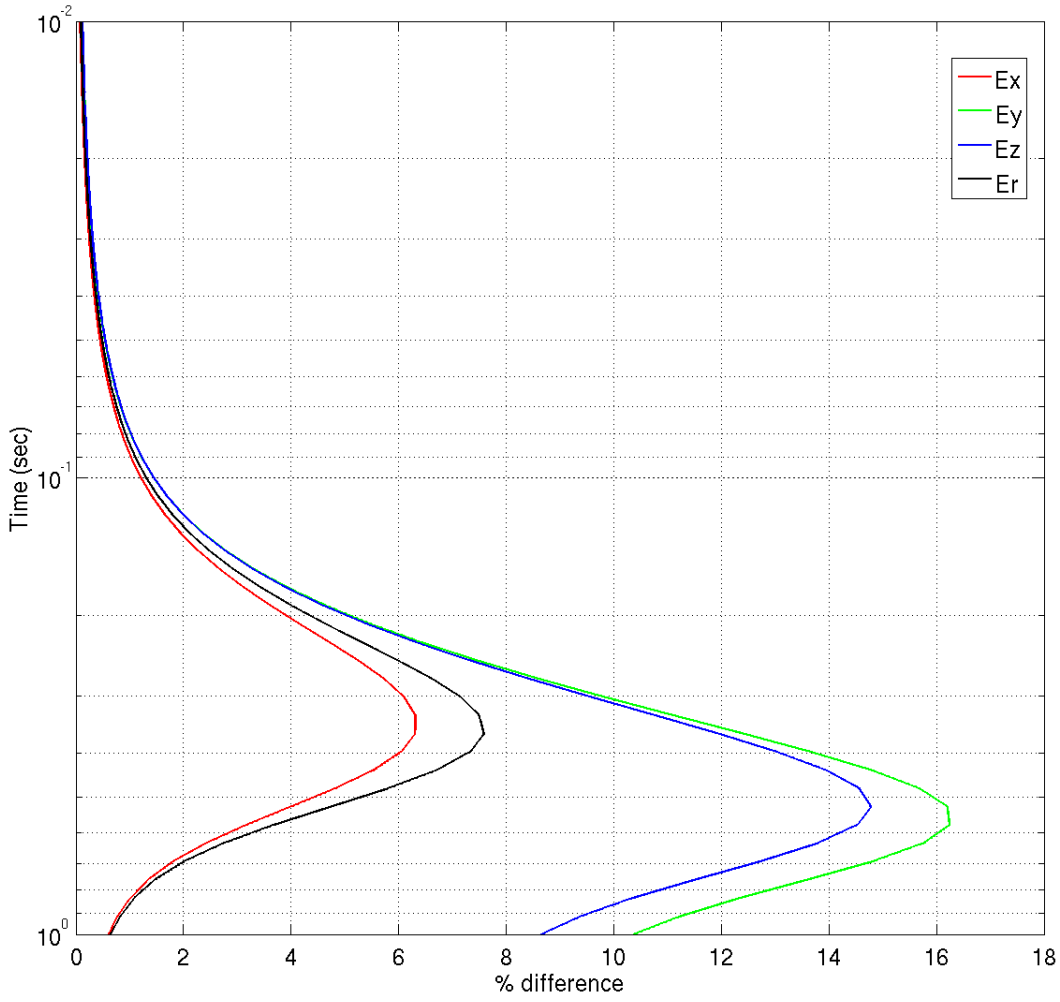

Figure 11. Percent difference for four E field components between model with and without the frac using the fine mesh with 12.22mm cells in the x and y directions including the steel casing. The receiver is at x=10, y=10 over the model shown in Figure 6 (10 Ωm background with 526 S/m frac) The source is a 30 A 50m x-directed dipole with (x, y, z) end points at coordinates (-25, 0, 0) and (+25, 0, 0). Ex is the field in the direction of the transmitter, Ey is orthogonal to x, Ez is vertical field and Er is the field in the radial direction between the transmitter mid-point and the receiver point.

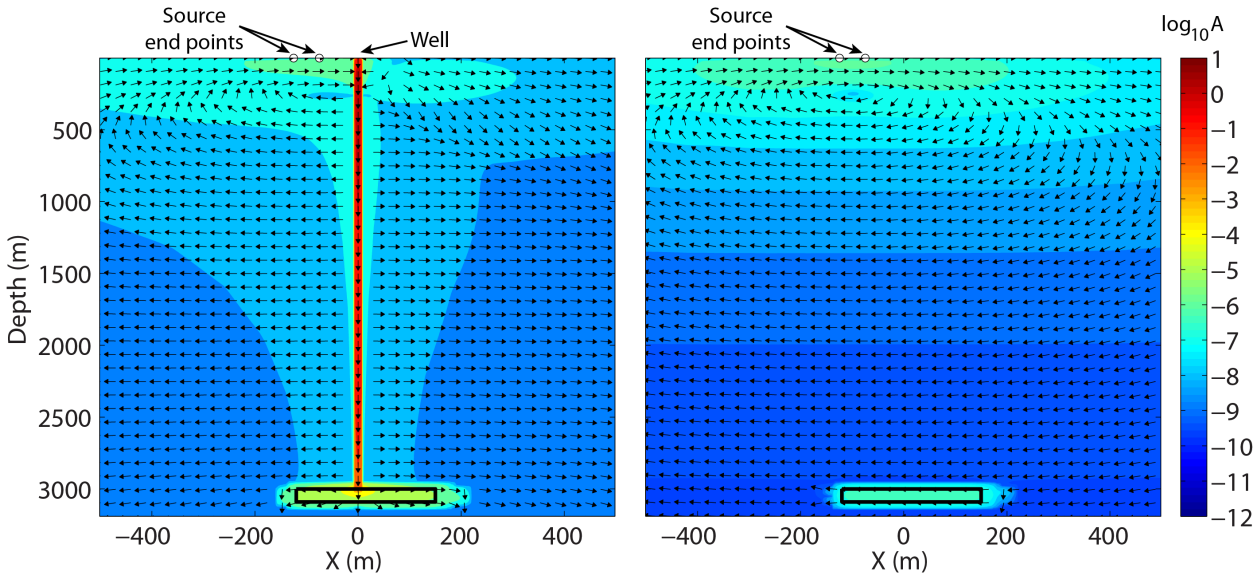

Figure 12. The electric current in the Y=0 plane of the transmitter and well at 0.001 sec after turn-off of the transmitter. The background resistivity is 10Ωm. The transmitter is a 50 m dipole source with 30 A centred at x = -100m, y =0. The frac geometry is shown in figure 6, the frac conductivity is 526 S/m. The colour scale is in $\log_{10}$ A, the arrows show current flow direction. The left panel shows the case with the steel casing included in the simulation and the right panel shows the case without the steel casing. Both calculations were performed on the same FD mesh shown in Figure 8. The maximum horizontal current at 0.001 seconds after turn off in the frac when the casing is included is 330 times larger than without the casing.

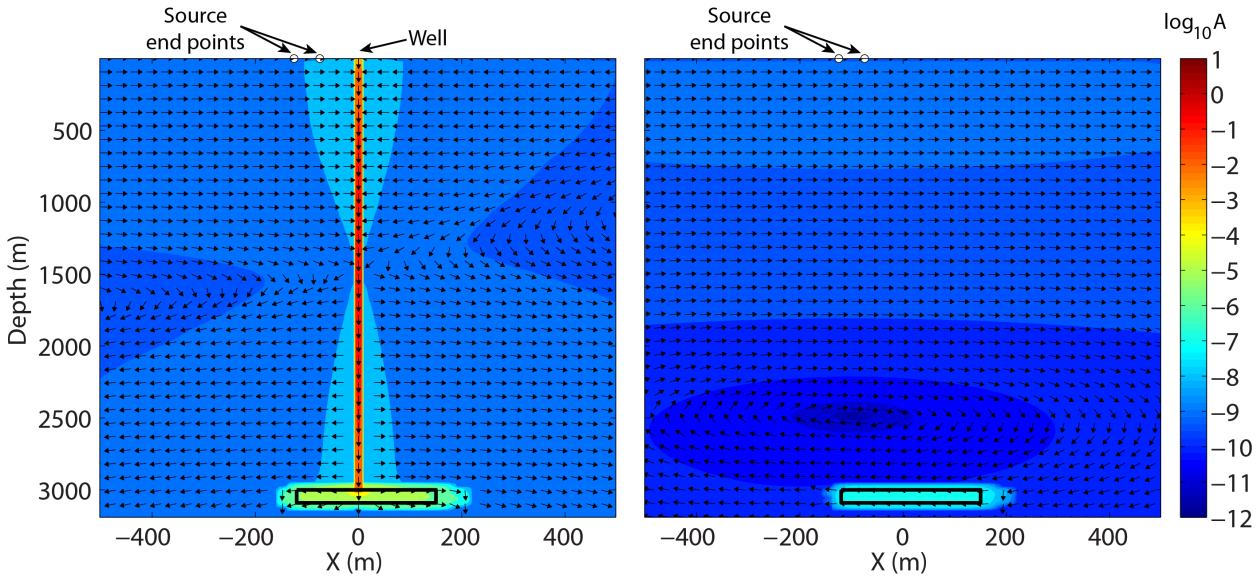

Figure 13. The electric current in the Y=0 plane of the transmitter and well at 0.1 sec after turn-off of the transmitter. The background resistivity is 10Ωm. The transmitter is a 50 m dipole source with 30 A centred at x = -100m, y =0. The frac geometry is shown in figure 6, the frac conductivity is 526 S/m. The colour scale is in $\log_{10}$ A , the arrows show current flow direction. The left panel shows the case with the steel casing included in the simulation and the right panel shows the case without the steel casing. Both calculations were performed on the same FD mesh shown in Figure 8. The maximum horizontal current at 0.1 seconds after turn off in the frac when the casing is included is 750 times larger than without the casing.

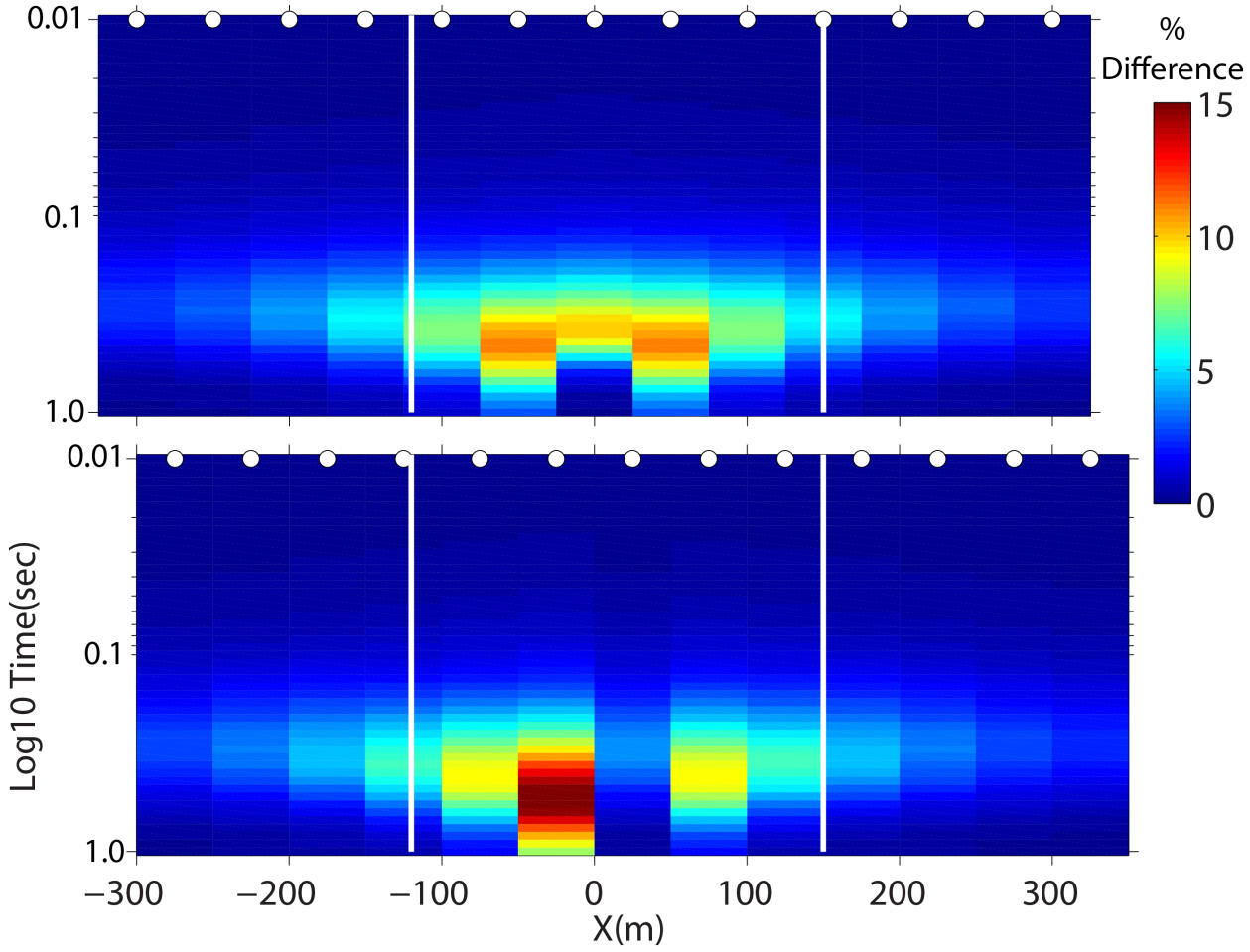

Figure 14. The percent difference between the before and after radial E measurements over a frac with dimensions 270 m x 90 m x 0.01222 m. The frac has conductivity 526 S/m (Figure 6) in a 10 Ωm background. Thirteen source-receiver pairs are used with a constant X direction source-receiver offset of 0m for a) and +50m for b). The line of receivers is at y=10m. The sources are centred every 50m from -300m to +300m. The percent difference at the midpoint between source and receiver colors each cell. The cell dimensions are the time and space increments of the data. The vertical white lines show the lateral extent of the frac (-120 to +150 m). The maximum difference is 11.1% for 0 X separation and 15.3% for +50m X separation. All fields are above the assumed E field noise floor of 3×10^{-10} V/m.

X separation (m)	0.01 S/m background			
	Proppant @ 526 S/m		Brine@ 30.5 S/m	
	% asymmetry	max %diff Er	%asymmetry	max %diff Er
0	14	172	0.12	20.3
10	15.5	175	1.7	20.2
25	35	182	3.6	20.8
50	95	213	10.1	23.6
75	130	230	14	24.7
100	152	258	16	27.1

X separation (m)	0.1 S/m background			
	Proppant @ 526 S/m		Brine @ 30.5 S/m	
	%asymmetry	max %diff Er	%asymmetry	max %diff Er
0	0.07	11.1	0.01	1.7
10	1.4	11.6	0.2	1.8
25	2.8	12.3	0.5	1.9
50	8.4	15.4	1.3	2.3
75	13	18.1	2	2.7
100	11	21	1.8	3.2

Table 3. Maximum percent difference with and without fracs and the maximum percent asymmetry in the percent difference patterns. Upper table is for 0.01 S/m (100 Ωm) background and lower table is for 0.1S/m (10 Ωm) background.

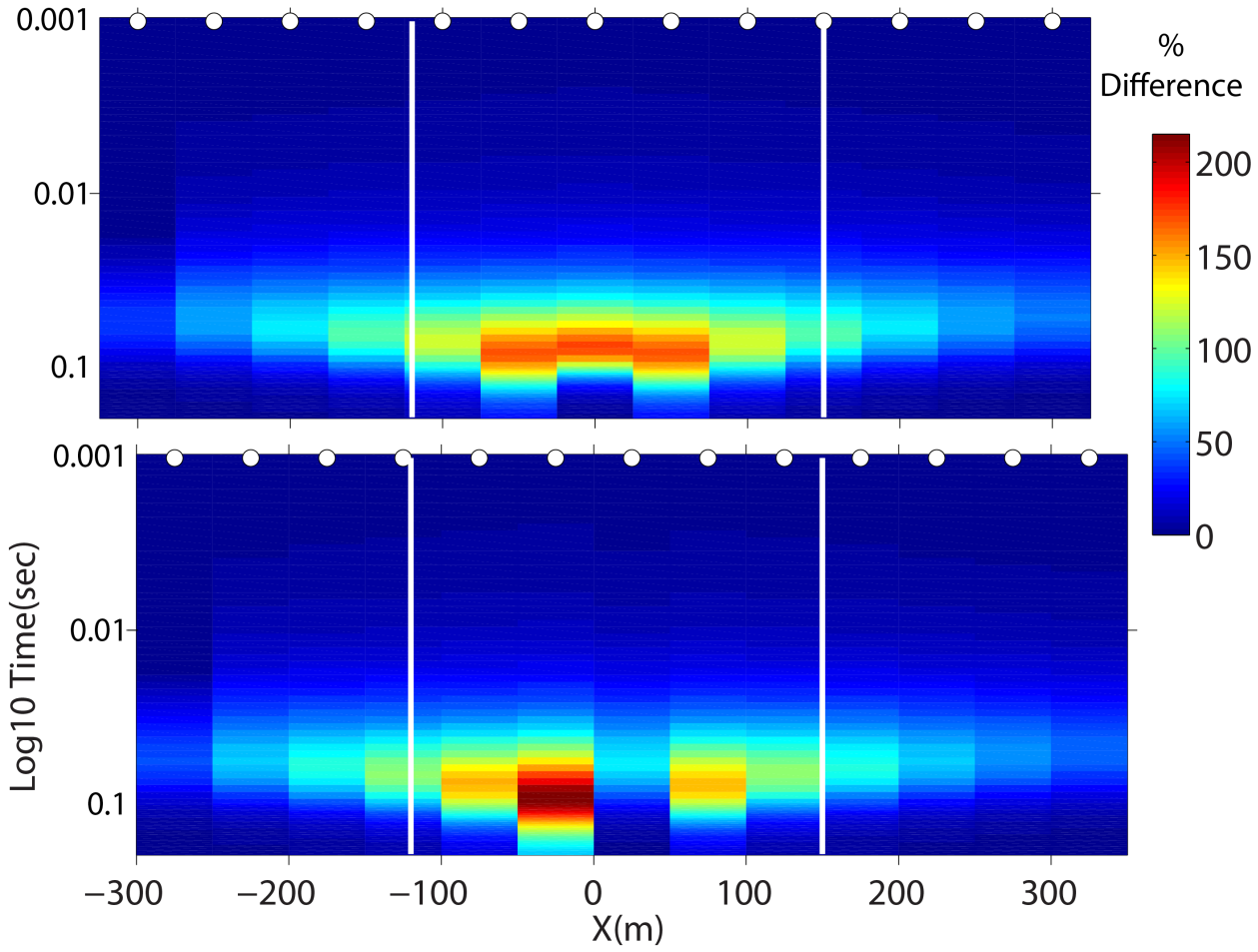

Figure 15. The percent difference between the before and after radial electric fields over a frac with dimensions 270 m x 90 m x 0.01222 m. The frac has conductivity 526 S/m (Figure 6) in a 100 Ωm background. Thirteen source-receiver pairs are used with a constant X direction source-receiver offset of 0m for a) and +50m for b). The line of receivers is at y=10m. The sources are centred every 50m from -300m to +300m. The percent difference at the midpoint between source and receiver colors each cell. The cell dimensions are the time and space increments of the data. The vertical white lines show the lateral extent of the frac (-120 to +150 m). The maximum % difference is 172% for 0 X separation and 213% for +50m X separation. . All fields are above the assumed E field noise floor of $3x10^{-10}$ V/m.

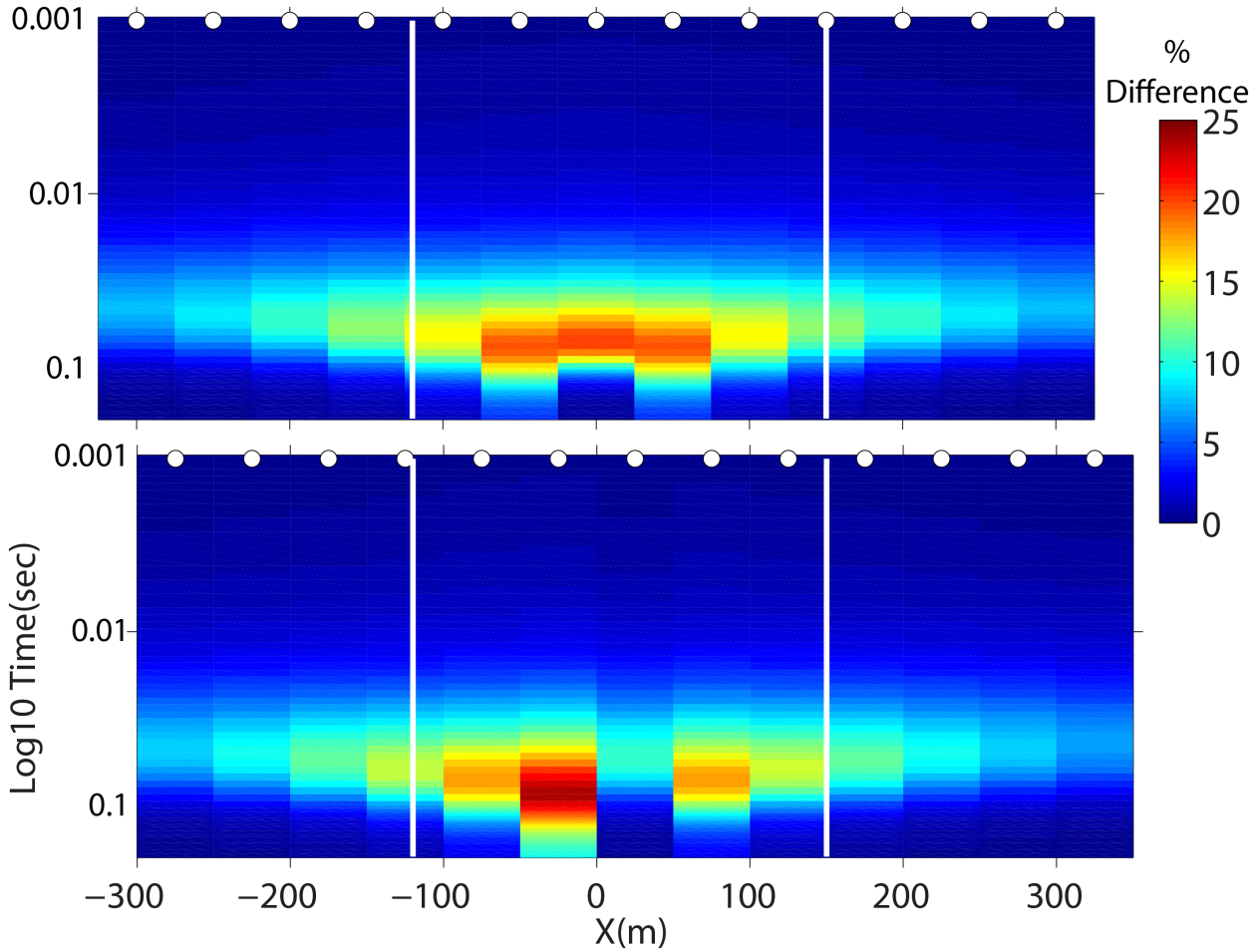

Figure 16. The percent difference between the before and after radial electric fields over a frac with dimensions 270 m x 90 m x 0.01222 m. The frac has conductivity 30.5 S/m (Figure 6) representing 100,000 PPM brine solution in a 100 Ωm background. Thirteen source-receiver pairs are used with a constant X direction source-receiver offset of 0m for a) and +50m for b). The line of receivers is at y=10m. The sources are centered every 50m from -300m to +300m. The percent difference at the midpoint between source and receiver colors each cell. The cell dimensions are the time and space increments of the data. The vertical white lines show the lateral extent of the frac (-120 to +150 m). The maximum % difference is 20.3% for 0 X separation and 23.6% for +50m X separation. All fields are above the assumed E field noise floor of $3x10^{-10}$ V/m.

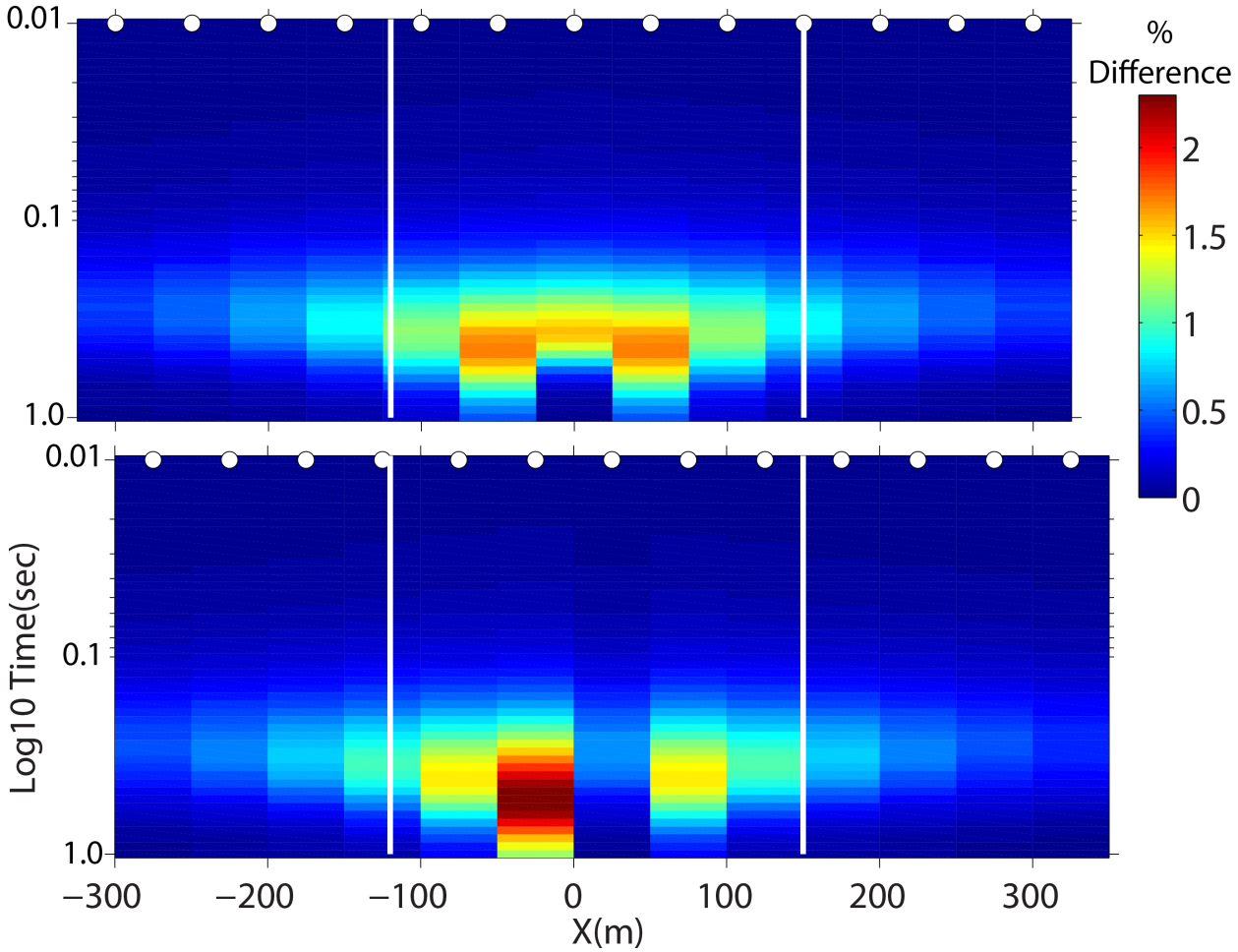

Figure 17. The percent difference between the before and after radial electric fields over a frac with dimensions 270m x 90m x 0.01222m. The frac has conductivity 30.5S/m (Figure 6) representing 100,000 PPM brine solution in a 10Ωm background. Thirteen source-receiver pairs are used with a constant X direction source-receiver offset of 0m for a) and +50m for b). The line of receivers is at y=10m. The sources are centered every 50m from -300m to +300m. The percent difference at the midpoint between source and receiver colors each cell. The cell dimensions are the time and space increments of the data. The vertical white lines show the lateral extent of the frac (-120 to +150 m). The maximum % difference is 1.7% for 0 X separation and 2.3% for +50m X separation. All fields are above the assumed E field noise floor of $3x10^{-10}$ V/m.